Modeling of gas-jet wiping at small standoff distances

A Gosset*, **P. Rambaud***, **L. Castellano***, **M. Dubois****, and **J –M Buchlin***
**von Karman Institute, Rhode-Saint-Génèse, Belgium*
***Arcelor Research, Ivoz-Ramet, Belgium*

Abstract

This paper presents a model to predict the jet wiping performance of a gas jet at small standoff distances. The pressure gradient and shear stress distributions induced by a 2D slot jet impinging on a flat plate is determined both by experimental and numerical methods for normalized standoff distances $L/d \leq 8$. . Correlations for the wiping actuators are proposed. They are implemented into a zero-dimensional analytical model which allows the prediction of the final film thickness after wiping h_f. The predicted values are compared with the data of wiping experiments conducted with water on a dedicated facility. An excellent agreement is obtained for jet Reynolds numbers lower than 4500. The results show that the final coating thickness remains almost constant as long as the normalized standoff distance does not exceed 7.

1 Introduction

The deposition of a very thin liquid film over a solid surface is the basis of many industrial-coating processes. After being deposited, the coating film solidifies, or dries out, leaving a protective layer for the substrate. This technique is used in hot-dip coating, in which the coating is a material in its liquid state, thus at very high temperature. The industrial requirements are such that the final coating thickness should be thin and uniform. For that purpose, the jet wiping technique allows the accurate control of the film thickness. It consists in a two-dimensional gas-jet impinging on the liquid layer withdrawn by the moving substrate. The excess coating flows down back to the dipping bath. The final thickness of the liquid film depends on several parameters such as the standoff distance L between the wiping nozzle and the substrate, the nozzle slot opening d, the substrate velocity V_P, the jet dynamic pressure P_n, and the physical properties of the fluid.

There is a particular interest in working at small standoff distances: smaller thickness can be achieved, at higher line velocity. The wiping performance is controlled by the upstream maximum pressure gradient of the jet at impingement on the solid surface, ∇P_{max}, and the maximum shear stress τ_{max}[1-2], as sketched in Figure 1. They both augment with the nozzle pressure. An alternative solution is to choose a small distance L between the nozzle and the solid surface. However, the behaviour of the wiping actuators $\nabla P_{\max}$ and τ_{max} is not well known in this confined mode, i. e. for $L/d \leq 8$. In this range indeed, the potential core of the jet may be modified over a distance by the presence of the impingement surface, or even directly interact with it (in the case of very short L/d), resulting in a specific evolution of ∇P_{max} and τ_{max}. Therefore it is worthwhile providing a model for the evolution of the wiping actuators in this range. Despite a few attempts[3-4] to characterize developing impinging jets, no effort has been spent so far to extract correlations for $\nabla P_{\max}$ and τ_{max}, and to validate them with the results of wiping experiments.

The aim of this paper is to develop a simple predictive model of gas-jet wiping in the case of normalized standoff distances $L/d \leq 8$. The methodology adopted is threefold: the distribution of the pressure gradient ∇P and the shear stress τ induced by the jet on a flat fixed plate are measured and compared to numerical simulations. Correlations of the wiping actuators ∇P_{max} and τ_{max} are established and inserted in an analytical jet-wiping model to predict the final film thickness h_f. The findings are then compared to the experimental data obtained on a dedicated facility.

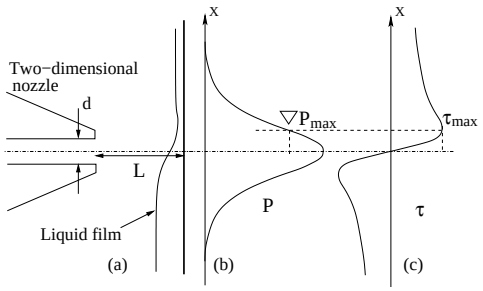

Figure 1: Sketch of the jet configuration: (a) Nozzle placement; (b) Typical impingement pressure profile; (c) Typical shear stress profile

2 Numerical simulations

Numerical simulations of the impinging gas jet on a flat plate are performed with the code Fluent 6.0. The simulations parameters are given and typical results are shown.

2.1 Mesh and boundary conditions

The computational domain is shown in Figure 2a. It is symmetrical and two-dimensional. The experimental conditions are simulated. The nozzle has an external angle equal to 50°, and three slot gaps are considered; d=0.7 mm, 1.4 mm and 2 mm. The width of the domain is 100 mm, which corresponds to x/d=50. The normalized standoff distance between the nozzle and the plate may vary from 2 to 8. A typical mesh layout is shown in Figure 2b. It is composed of hybrid non-structured elements, quadrilaterals in the near-wall region, and triangular in the far-wall field. Very fine grid clustering close to the wall is required to extract accurately the pressure gradient and the shear stress. Only half of the domain is simulated because of the flow symmetry. The typical number of computational cells is 150000. The boundary conditions are the velocity distribution at the exit of nozzle and the pressure outlet for the circular boundary in the ambient air. The impingement plate and the nozzle sides are regarded as impermeable walls.

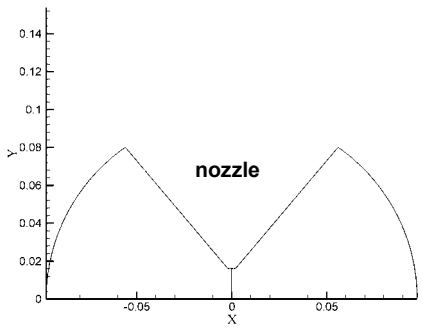

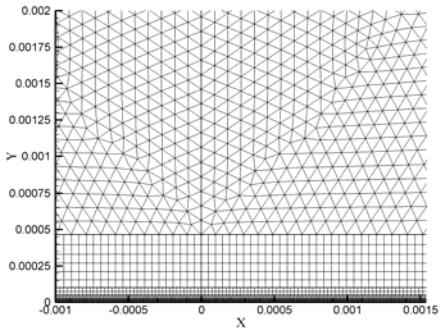

Figure 2

(a) Domain geometry for L/d=8. The dimensions are in meters.

(b) Close-view of the mesh at 1d from the stagnation point (x=0, y=0)

2.2 Simulation parameters

Since the quantities to be sought for are the pressure and the wall shear stress, the mesh is designed to solve the flow up to the viscous sublayer, which is estimated to be few microns high. Since we are only interested in mean values, a RANS model is adopted instead of Large Eddy Simulation, disregarded in this study due to its time cost. The k-ε turbulence model is used in its Realizable version. The initial version of this model, so-called standard k-ε, uses for closure the hypothesis that the first cell at the wall lies in the equilibrium layer where the production of k and ε are in equilibrium; it will be therefore avoided, as well as logarithmic wall

functions. The k-ε Realizable allows avoiding the non-physical results obtained when the mean velocity gradient (thus the shear stress) is too high. One of the k-ε constants C_μ is made variable[5], and sensible to the velocity gradient and turbulence. Shih et al.[6] apply this idea, and replace the ε equation of the initial model by a transport equation of the square of vorticity fluctuations.

The numerical schemes are 2nd order upwind, and the solver is used in double precision. In order to point out the influence of parameters such as the velocity profile at the exit of the nozzle and the initial turbulence intensity level, several computations are performed for a nominal standoff distance L/d=8. Top-hat and developed velocity profiles are tested. The top-hat profile is a uniform velocity profile across the width of the slot, while the developed profile is computed from the experimental data of Maurel[7]. The value of the turbulence intensity TI at the exit of the nozzle is fixed to 1%, 10% and 20%, respectively. Simulations are also conducted for L/d=2, 4, 6, and 8 with the appropriate corresponding meshing, and turbulence intensities of 0.1% and 10%.

2.3 Results

The final normalized residuals are found to be exceptionally low (of the order of 10^{-9} in the less converged simulation). This good degree of convergence is attributed to the mesh quality in the near-wall region, but also to the use of the solver in double precision.

The normalized pressure gradient distribution obtained for different inlet velocity profiles and TI-values is plotted in Figure 3a for L/d=8 and a jet Reynolds number Re_j=4500 (based on the nozzle slot opening d and the jet exit velocity U_0). The degrading effect of the initial turbulence on the pressure gradient can be depicted: the peak value decreases of 20% when the initial turbulence augments from 1 to 10%. Moreover, the location of the peak is shifted of 28% away from the stagnation point in terms of x/d. This is probably due to the reduction of the potential core length caused by the higher initial turbulence level[7], which accelerates the mixing layer formation at the edges of the jet. On the other hand the initial turbulence level does not affect much the development of the wall jet. Comparatively, the velocity profile has a much weaker effect on the evolution of the pressure gradient.

The corresponding wall shear stress distribution is plotted in Figure 3b. As for the pressure gradient, the shear stress lessens as the initial turbulence intensity increases. Now the inlet velocity profile has a more important effect: the "ideal" (top-hat) profile gives higher values than the developed profile. The difference reaches 12% at the peak value, for TI=20%. Since the wall shear stress is a velocity gradient quantity, it can be inferred that the initial velocity gradient at the exit of the jet, which is lower in the case of a developed profile, involves a lower gradient after the deflection of the flow in the stagnation region.

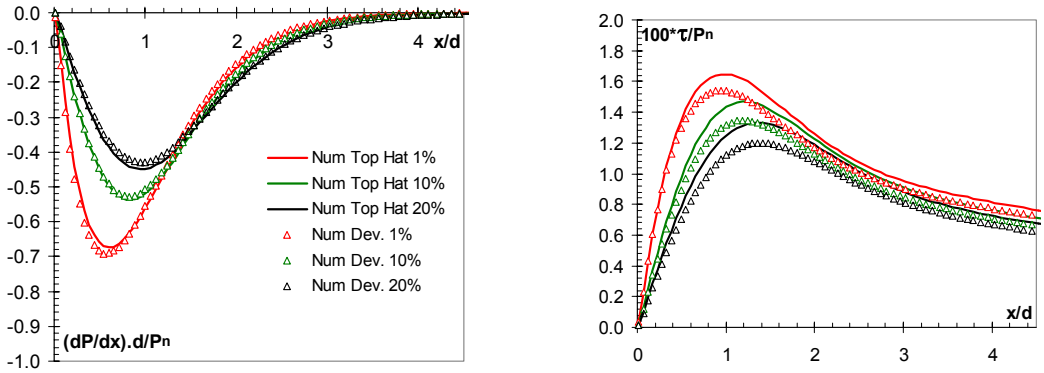

Figure 3: Results of Fluent simulations for L/d=8, Re_j=4500

(a) Normalized pressure gradient at the wall (b) Normalized wall shear stress

3 Experimental approach

Experimental measurements are conducted in order to provide a database to establish correlations for ∇P_{max} and τ_{max}, as well as a validation of the numerical results.

3.1 Facility

The experimental approach is discussed in [8], therefore it will not be described into details here. The setup is sketched in Figure 4. It consists in a 2D slot nozzle impinging normally on a plate mounted on a displacement system 2 μm accurate. The plate is instrumented with a 0.5 mm diameter static pressure tap, while the shear stress is measured with the so-called razor-blade technique explained in[8]. It uses simplified Stanton tubes formed by a razor blade located over a pressure hole. The size of the probe in this case is 75 μm and the blade is 150 μm thick. The uncertainty analysis related to this technique is also reported in [8]. The static pressures are measured by a membrane pressure transducer; and the signal is acquired at 2 kHz on a Personal Computer. The spatial step for the profiles is 0.1 or 0.2 mm, depending on the nozzle width. The nozzle geometry is the same as the one described in [8]. A 14 kW centrifugal blower produces the air flow. The turbulence level at the exit of the jet is measured with a hot wire (7.5 kHz frequency response) located at the centre of the nozzle. The turbulence intensity is 1.1% at 1 mm and 1.5% at 2 mm from the nozzle lips, respectively. Although the hot wire might be intrusive for a nozzle slot opening d=1.4 mm, the order of magnitude of the turbulence level can be considered as representative.

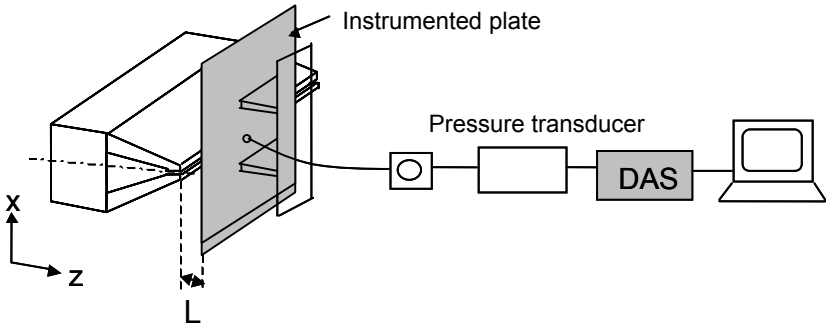

Figure 4: Sketch of the experimental setup

3.2 Results

- **Validation of numerical simulations**

Despite the use of a computationally cheap model, the wall pressure gradient is well captured in amplitude (Figure 5a), considering that the measured *TI* was about 1%. However, the $\nabla P_{max}.d/P_n$ peak location is poorly predicted by the numerical simulations. Such a discrepancy results from the turbulence model adopted. Two equations models are known to have difficulties in predicting stagnation flows. This drawback has already been emphasized by Durbin[9,10] and Behnia et al[11]. Indeed, the same exercise repeated through LES simulation leads to an excellent agreement with experiments[8].

As far as the shear stress is concerned, the location of the peak is closer to experimental results, as depicted in Figure 5b. The profiles compare qualitatively well, but the experimental values are systematically lower than the numerical ones. This drift might result from the effect of the physical size of the Stanton probe (razor blade), which tends to underestimate the value of wall shear stress. Moreover, it is worth noting that the probe calibration is conducted in a fully developed turbulent channel flow with zero pressure gradient, which in essence is rather different from that of an impinging jet. In the latter indeed, the stagnation zone may be partially laminar, because of the strong favorable pressure gradient[4,12]. This pressure gradient effect tends

to counteract the underestimation due to the probe size[12]. These antagonist sources of error make it difficult to appraise the complete validation of the numerical simulations. In any case, the pressure gradient flow conditions in the stagnation region (x/d<1) are beyond the recommendations of Patel[13] for a maximum uncertainty of 6%. We can therefore expect much higher experimental uncertainties on the shear stress.

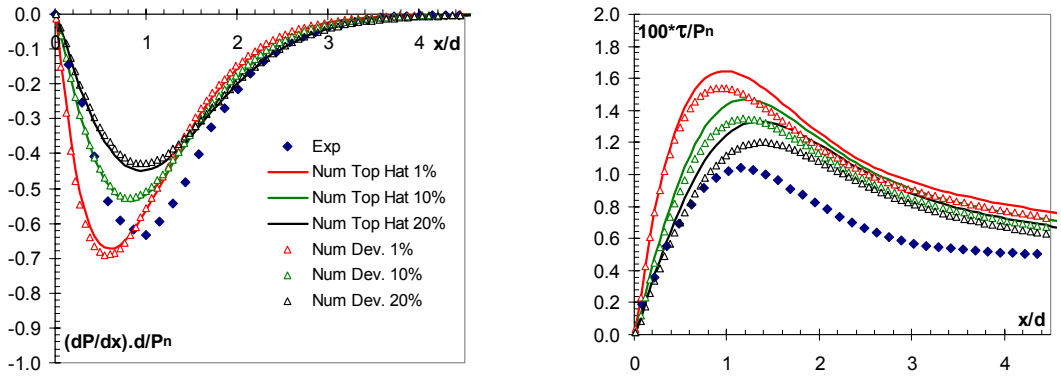

Figure 5: Fluent simulations and experimental data comparison : L/d=8, Re_j=4500

(a) Pressure gradient at the wall (b) Normalized wall shear stress

Based on a laminar boundary layer hypothesis in the stagnation zone, Phares et al.[4] develop a theoretical model for the maximum shear stress in the case of L/d≤8. For that purpose, they calculate the different flow regions independently, with the respective appropriate approximations for Navier-Stokes equations (free jet, non viscous impacting flow, impingement boundary layer and wall jet regions). This model gives a τ_{max}/P_n value of 0.0153 for L/d=8, while the present numerical simulations predict values between 0.0135 and 0.0165. This good agreement supports the physical intuition that the maximum shear stress is located in a laminar boundary layer region, at least in the present conditions.

- **Pressure gradient correlation**

Typical pressure distributions obtained experimentally for 2≤L/d≤8 are presented in Figure 6a. The jet Reynolds number is 4500, while the nozzle gap is d=1.4 mm. For these L/d values, they can be approximated by the following expression, which does not depend on the jet Reynolds number within the range considered (2700≤ Re_j ≤6800):

$$\frac{P}{P_{\max}} = (1 + 0.5\xi^{3.3})^{-1.34} \tag{1}$$

where ξ=x/b. b is the location of $P_{max}/2$ with respect to the jet axis. Then differentiating equation (1) leads to the following pressure gradient correlation:

$$\frac{d}{d\xi}\left(\frac{P}{P_{\max}}\right) = -2.211\xi^{2.3}(1 + 0.5\xi^{3.3})^{-2.34} \tag{2}$$

The corresponding curve is shown in Figure 6b. The maximum dimensional pressure gradient is thus given by the following expression:

$$\nabla P_{\max} = -0.862\frac{P_{\max}}{b} \tag{3}$$

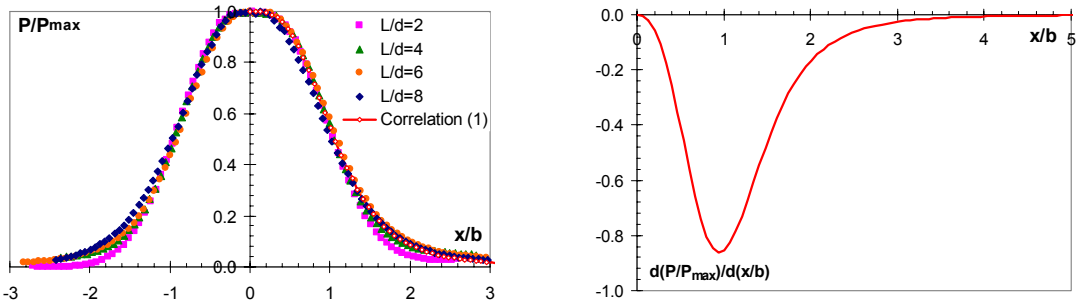

Figure 6

(a) Typical experimental pressure profiles (Re_j=4500, d=1.4 mm)

(b) Pressure gradient correlation

The evolutions of P_{max}/P_n and b/d are found to be independent of the jet Reynolds number between 2700 and 6800, and they can be modeled by the following expressions (Figures 7a and 7b):

$$L/d \le 5: \quad \frac{P_{\max}}{P_n} = 0.98 \qquad \frac{b}{d} = 0.086\frac{L}{d} + 0.9834 \tag{4}$$

$$5 < L/d \le 8: \quad \frac{P_{\max}}{P_n} = 0.01\left[-1.1947\left(\frac{L}{d}\right)^2 + 11.962\frac{L}{d} + 68.27\right] \qquad \frac{b}{d} = 0.0181\left(\frac{L}{d}\right)^2 - 0.1927\frac{L}{d} + 1.533 \tag{5}$$

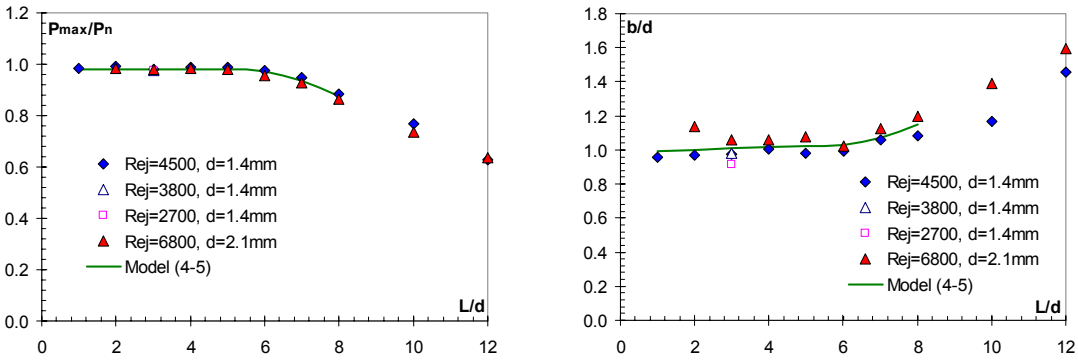

Figure 7

(a) Evolution of the normalized P_{max} with L/d

(b) Evolution of the normalized b with L/d

The model thus obtained for the normalized maximum pressure gradient $\nabla\hat{P}_{\max} = \nabla P_{\max}.d/P_n$ is compared to the one of Tu and Wood[3], and to the numerical data in Figure 8. Tu and Wood provide a very complete set of wall pressure and shear stress measurements beneath a plane impinging jet, for wide range of L/d between 2 and 20. Correlations for $\nabla P_{\max}$ and τ_{max} can easily be derived from their database. The present experimental correlation exhibits the same trend as the model of Tu et al., characterized by a plateau type behaviour up to L/d=6, and a smooth transition over $6 \le L/d \le 8$, where the dependence of the pressure gradient on the distance L/d is still weak. This plateau is certainly related to the behaviour of the potential core of the jet, although it is quite longer (6d). Indeed, depending on the turbulence intensity, the numerical simulations give potential core lengths ranging between 1.5d and 5d for L/d=8 (the core length

is estimated as the distance at which the velocity on the jet axis is 99% of the maximum). For larger standoff distances, the ∇P_{max} evolution with L/d coincides with the pioneer relation of Beltaos[13] for a developed impinging jet ($L/d \geq 8$):

$$\nabla P_{max} = B \frac{P_n . d}{L^2} \tag{6}$$

where B is a coefficient depending on the nozzle geometry.

In the range $2 \leq L/d \leq 8$, the proposed correlation yields values 12% larger than Tu's data. Several reasons may be invoked to explain such a discrepancy: a difference in the nozzle geometry and/or in the initial turbulence level (both not specified in [3]). The Fluent simulations lead to a monotonic decrease of the pressure gradient and a highly overestimated value for strong confinements (L/d=2). Such a result might be attributable to the artificial confinement produced by the too close boundaries of the numerical domain and/or by a less inflow entrainment, as suggested by Babu and Mahesh[14].

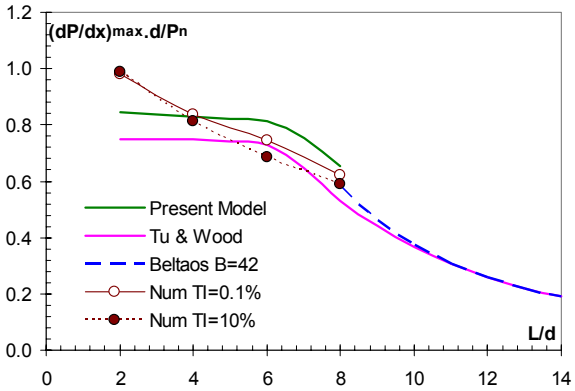

Figure 8: Comparison of experimental and numerical correlations for the maximum pressure gradient as a function of L/d

- **Shear stress correlation**

Typical shear stress profiles obtained experimentally are shown in Figure 9, for Re_j=4500 and d=1.4 mm. It is observed that the peak position moves slightly from the jet axis as L/d increases.

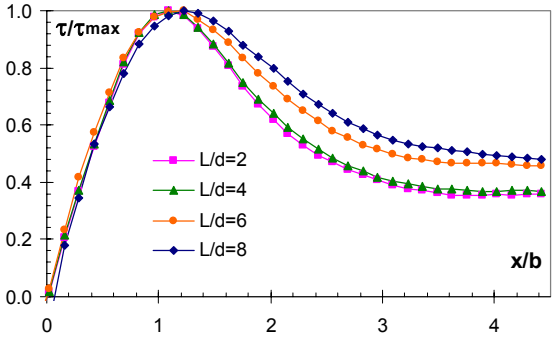

Figure 9: Typical experimental shear stress profiles (Re_j=4500, d=1.4 mm)

The normalized maximum shear stress $\hat{T}_{max} = (\tau_{max} . L/d)/P_n$ is plotted in Figure 10a. Up to L/d=8, its evolution is linear, and dependent on the jet Reynolds number. It can be modeled by the following equation:

$$100\frac{\tau_{\max}.L/d}{P_n} = a\frac{L}{d} + b \tag{7}$$

where coefficients a and b are expressed in function of Re_j:

$$\begin{aligned} a &= 3.83\,\mathrm{Re}_j^{\,2} - 4.58\,\mathrm{Re}_j + 2.21 \\ b &= -2.13\,\mathrm{Re}_j^{\,2} + 2.55\,\mathrm{Re}_j - 0.18 \end{aligned} \tag{8}$$

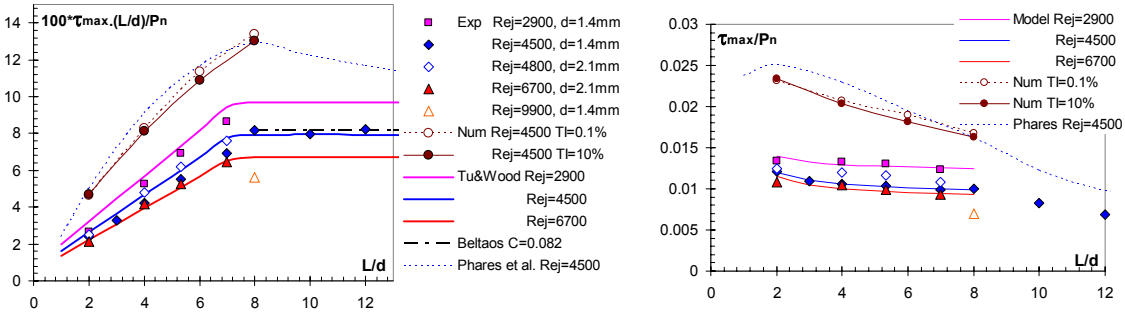

Figure 10

(a) Evolution of normalized $\hat{T}_{\max}$ with L/d

(b) Evolution of T_{max}/P_n with L/d (experimental data)

The resulting shear stress correlation is in good agreement with the correlation proposed by Tu and Wood[3] (Figure 10a), who used Stanton probes similar to ours, although slightly thinner (100 µm instead of 150). They show that an augmentation of the physical size of the probe leads to an underestimation of the shear stress, which supports the fact that their values are slightly higher than the present data. The normalized shear stress seems to tend towards an asymptotic behaviour for Re_j>7000, as also found by Tu et al. They argue that this might be related to transition in the developing wall jet, but this trend could also result from a more important error due to the probe size effect when Re_j increases. For L/d≥8, the values converge towards the model of Beltaos[13]:

$$\tau_{\max} = C\frac{P_n.d}{L} \tag{9}$$

where C is also a coefficient depending on the nozzle geometry. Typically, it is found that C=0.082 for Re_j=4500.

The plot in Figure 10b presents the same data as in Figure 10a, but it figures out the existence of a shear stress plateau up to L/d=8. The maximum shear stress values extracted from the numerical simulations are 65% to 90% higher than the experimental data, as L/d decreases from 8 to 2. But these numerical results are in very good agreement with the theoretical predictions of Phares et al.[4], which reinforces the hypothesis of a laminar boundary layer in the stagnation region of the jet. The difference observed with the experimental results explained in details in a previous paragraph. On a numerical point of view, the viscous sublayer is estimated to be 3 µm thick at the peak location, which is within the mesh resolution at the wall. However, the impinging jet flow is very particular because of its change of direction and re-acceleration, which implies a very thin boundary layer. Because of the strong favourable pressure gradient, the logarithmic wall law is not valid in the stagnation region, and a precise computation including the laminar sublayer is required. The numerical estimation of shear stress is therefore a challenging task.

The wiping actuators have been experimentally characterized, and correlations are proposed for their evolution in the range $2 \le L/d \le 8$. These correlations compare well with data from literature, when the same type of shear stress probe is used. They will be implemented in an analytical wiping model described in section 4. The numerical results reveal some discrepancy, although they are in agreement with theoretical predictions assuming a laminar boundary layer in the stagnation zone.

4 Jet wiping Modeling

4.1 Mathematical formulation

Several models for the film interface in jet wiping are proposed in the literature with different levels of solutions[1-2,15-16]. The details of the derivation will therefore not be developed here, only the main features are emphasized.

The theoretical description of gas-jet wiping usually relies on the lubrication approach, which assumes negligible inertia with respect to viscous, gravity and pressure terms. The (Ox) momentum equation of the film states that the shear stress balances the weight and pressure, and the associated boundary conditions express the no-slip condition of the film on the substrate, and the continuity of shear stress at the free surface. The resulting flow rate equation has the following non-dimensional form:

$$\Gamma \frac{d^3 \hat{h}(X)}{dZ^3} = 1 + \nabla \hat{P}(X) + \frac{2Q - 3\hat{h} - 1.5\hat{T}\hat{h}^2}{\hat{h}^3} \tag{10}$$

where $\nabla \hat{P}$ and $\hat{T}(X)$ are respectively the pressure gradient and shear stress distributions of the jet at impingement. $\hat{h}$ and Q are the local film thickness and flow rate. The normalized variables are defined as follows: $X = x/d$, $\hat{h} = h/h_0$ with $h_0 = \sqrt{\mu_1 U/\rho_1 g}$, $\Gamma = \sigma h_0/\rho_1 g d^3$, $Q = q/q_0$ with $q_0 = 2/3.V_P h_0$, $\nabla \hat{P} = \nabla P/\rho_1 g + 1$, and $\hat{T} = \tau/\tau_0$ with $\tau_0 = \sqrt{\mu_1 V_P \rho_1 g}$. Subscript 0 refers to the dragged liquid film without jet wiping, and 1 refers to the liquid phase properties.

Equation (10) has two unknowns, $\hat{h}$ and Q, and the continuity equation is needed for its solving. A simplified model can be derived from (10), assuming a negligible effect of the surface tension:

$$(1 + \nabla \hat{P})\hat{h}^3 - 1.5\hat{T}\hat{h}^2 - 3\hat{h} + 2Q = 0 \tag{11}$$

The solution of (11) is obtained by solving locally the cubic equation, using the pressure gradient and shear stress distributions $\nabla \hat{P}$ and $\hat{T}(X)$ obtained experimentally or numerically.

A zero-dimensional model (hereafter referred to as the Knife Model) can be derived from (11) if one postulates that the wiping mechanism is the result of the first maximum jet pressure gradient and maximum shear stress. This approach assumes implicitly that both quantities act at the same location X_{opt} (which is very close to reality[2]) and that surface tension has no effect on the final film thickness. With such an approximation, the film equation reduces to the simple algebraic equation:

$$(1 + \nabla \hat{P}_{\max})\hat{h}_{opt}^{\ 3} - 1.5\hat{T}_{\max}\hat{h}_{opt}^{\ 2} - 3\hat{h}_{opt} + 2Q_{opt} = 0 \tag{12}$$

Since there are two unknowns, $\hat{h}_{opt}$ and Q_{opt}, a second equation is needed. It is derived by stating that the wiping efficiency corresponds to the optimum final net flow rate, so that:

$$\hat{h}_{opt} = \frac{\hat{T}_{\max} + \sqrt{\hat{T}_{\max}^2 + 4(1+\nabla\hat{P}_{\max})}}{2(1+\nabla\hat{P}_{\max})} \tag{13}$$

Once the flow rate Q is determined from (12), the final film thickness h_f is readily obtained.

4.2 Experimental facility

The jet wiping experiments consist in measuring the mean film thickness after wiping. The test facility which was used for that purpose is shown in Figure 11. It includes a vertical rubber strip 5 m long and 0.5 m wide, stretched between two rolls. The wiping nozzle is the same as the one described in Figure 3. The strip is set into motion by the upper roll, which is entrained by an electric motor. The strip velocity, which can be adjusted precisely in the range 0.5 to 5 m/s, is measured by means of a tachometer. The lower roll is fixed to a mechanical displacement system allowing the adequate stretching of the strip. It dips into a bath of water to which a small concentration of surfactant was added, to ensure a good wettability of the strip. The surface tension of the water drops to 0.03 N/m. The nozzle is positioned 0.8 m above the free surface of water and perpendicularly to the strip. The 0.6 m nozzle is sufficiently long to avoid edge effects, and it is fed up to 8 kPa with a blower similar to the one mentioned before. A calibrated Validyne pressure transducer measures the pressure in the nozzle chamber. For sake of simplicity, the wiping mechanism is studied only on one side of the strip. To ensure a good stability of the strip in the impact region of the jet, the rear face is sliding on an aluminium plate lubricated by the entrained water. The distance L between the nozzle and the strip is tuned using shims. The liquid film mean thickness h_f is determined through the flow rate measured by weighting the liquid collected at the top of the strip during a time elapse. The film is indeed withdrawn at the top of the band by the action of a rubber scraper combined to a vacuum cleaner which is based on 4 bars air ejectors. Two lateral small jets draw the liquid film towards two suction ports which are connected to a cyclone. A balance measures the amount of the collected water while the weighting time is controlled by a chronometer. The measurements of the film thickness h_f after wiping are reproducible within 3% in average, which is the order of magnitude of the uncertainty on h_f.

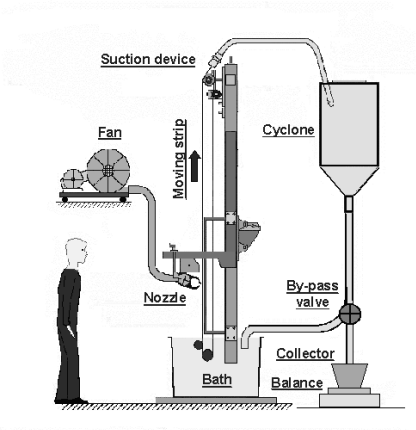

Figure 11: Gas-jet wiping facility

4.3 Validation

The correlations of the wiping actuators ∇P_{max} and τ_{max} are now inserted in the 0D Knife model. The aim is to verify that the film thicknesses can be adequately predicted in the confined gas-jet regime.

Experimentally, the evolution of the film thickness h_f with L/d is measured for $2 \leq L/d \leq 12$. All wiping parameters are kept constant. The substrate velocity is fixed to 1.53 m/s. Three nozzle gaps are tested: d=0.7, 1.4 and 2.1 mm. For each slot, the nozzle pressure P_n is adjusted so that $h_f \approx 17$ μm for L/d=2 and then it is kept constant throughout all the tests. The corresponding jet Reynolds numbers are 2100, 4500 and 7400, respectively.

Figures 12 to 14 show that in the three cases, a wiping plateau is observed. In this region, which extends up to L/d ≈7 (well beyond the jet potential core length) the film thickness is almost independent of L/d. For L/d>8, the thickness curve has a steeper slope, which is characteristic of the jet development in the far field[13].

This film thickness behaviour is the reflection of the evolution of the wiping actuators in confined mode. The maximum pressure gradient is constant until L/d=5, and it undergoes a transitional decrease for L/d between 6 and 8, in which the dependence of h_f on L/d is weaker than in the fully developed mode (L/d>8). Likewise, the maximum shear stress decreases very slightly until L/d=8, almost forming a plateau (Figure 10b). As depicted in Figure 12 for Re_j=4500, the values predicted by the 0D model completed with the experimental closure correlations compare well with the jet wiping measurements. They are also in agreement with the predictions obtained when the correlations of Tu and Wood[3] are used. The predictions obtained when the effect of the shear stress is omitted shows that its influence cannot be neglected. The predicted final film thickness is in average 40% higher. In the confined mode, the Knife model turns out to be a bit more sensitive to the pressure gradient than to the shear stress: an increase of 20% increase of ∇P_{max} involves a h_f decrease of 6.5%, while a similar increase of τ_{max} results only in a decrease of 5%.

The maximum pressure gradient and shear stress obtained from the numerical simulations yield an underestimation of the final film thickness. This is due to the higher values found for the shear stress. As expected, the predictions based on the shear stress model of Phares et al.[4] are in good agreement with the numerical results. The thickness plateau is not so obvious; that can be explained by the monotonic decrease of ∇P_{max}.

The same exercise is repeated for two different Reynolds numbers: Re_j=2100 with d=0.7 mm in Figure 13 and Re_j=7400 with d=2.1 mm in Figure 14. Figure 13 shows that for the lowest Reynolds number, the Knife model predictions are in excellent agreement with measurements. The model of Phares leads to an underestimation of the film thickness, probably due to the non adequacy of the model for such low Reynolds number. On the other hand, Figure 14 points out that for Re_j=7400, the correlations proposed here lead to an overestimation of 25%. At this higher Reynolds number, the jet-correlation proposed by Tu and Wood[3] does not provide better results either. To explain this discrepancy, two sources of error can be identified. The first one lies in the concept of the Knife model itself which, by assuming the same location for ∇P_{max} and τ_{max}, tends to predict systematically a smaller final thickness. The second one is the possible underestimation of the wiping actuators at high jet Reynolds number; ∇P_{max} alone would need to be 50 to 110% higher to obtain predictions in agreement with measurements, and τ_{max} alone would need to be 40 to 75% higher. The experimental estimation of τ_{max} could possibly reach uncertainties of this order of magnitude, because of the measurement technique used, which becomes probably more inaccurate as Re_j rises (the higher is the Reynolds number, the thinner is the boundary layer in the stagnation zone of the jet). The model of Phares provides good results (it is probably the good Re_j range for it to be applied), and this reinforces the hypothesis formulated before that the Stanton probe measures erroneous shear stress at higher Re_j.

The final film thickness predicted by the Knife model is thus affected by a combination of possible errors, and it is hard to know how they compensate each other. The crucial effect of the shear stress is demonstrated here, and a precise estimation of the latter is required for a reliable wiping model. The confrontation of the Knife model output with the results of wiping experiments allows figuring this problem. Further uncertainty analysis of the shear stress measurements is particularly needed for a clarification of the Re_j-effect. The discrepancy

between experimental and predicted h_f values for Re_j=7400 cannot be attributed to a single cause.

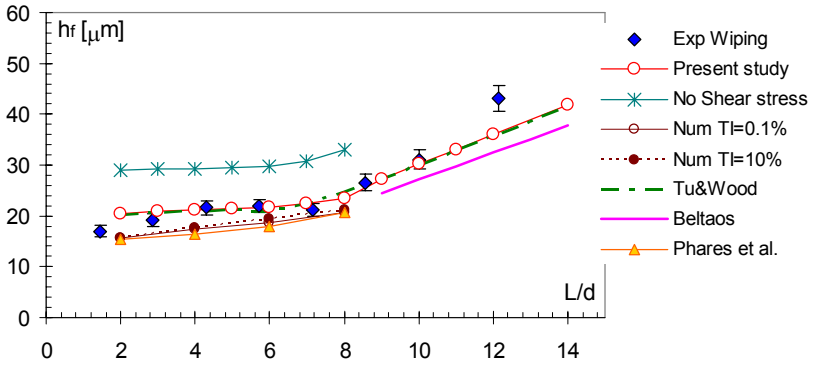

Figure 12: Comparison of jet wiping measurements with Knife model predictions based on experimental and numerical correlations for ∇P_{max} and τ_{max} (Re_j=4500, d=1.4 mm)

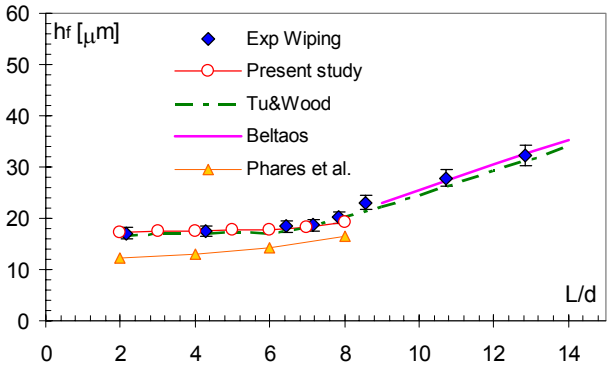

Figure 13: Comparison of jet wiping measurements with Knife model predictions for Re_j=2100 and d=0.7 mm

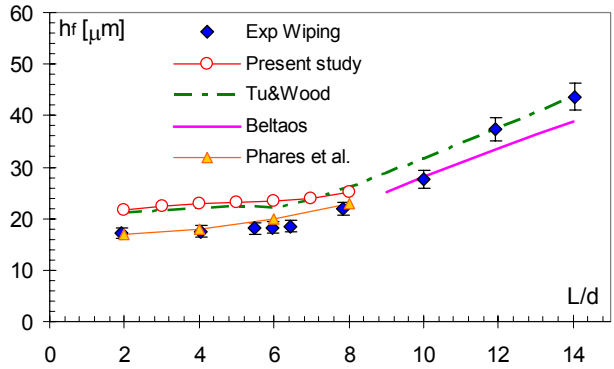

Figure 14: Comparison of jet wiping measurements with Knife model predictions for Re_j=7400 and d=2.1 mm

5 Conclusions

The jet wiping process for small standoff distances is studied through theoretical, numerical and experimental approaches.

The methodology consists first in characterizing the wiping actuators produced by the impinging gas jet. Correlations are proposed for the evolution of the maximum pressure gradient and shear stress with the normalized standoff distance in the range $2 \leq L/d \leq 8$. They compare qualitatively well with numerical simulations

The jet correlations are then implemented in an analytical zero-dimensional model ("Knife model") developed for the prediction of the film thickness. The wiping predictions are compared to experimental data obtained on a dedicated facility. For lower jet Reynolds numbers $Re_j \leq 4500$, the Knife model, based on the ∇P_{max} and τ_{max} correlations found experimentally provides very good predictions for the final film thickness. The operating window exhibits a plateau of the film thickness for L/d ranging from 2 to 7. Such a finding is of great interest for practical applications, because a small variation of L due to substrate vibration results in a negligible variation of the coating thickness.

This study is a first step in the applicability of the Knife model in industrial jet wiping, in confined mode. However, further study is needed for the validation of the model at higher Reynolds numbers ($Re_j > 7400$), like it is usually the case on industrial lines, e.g. galvanization lines.

6 References

1. Ellen, C. H., Tu, C. V., 1984, An analysis of Jet Stripping of Liquid Coatings, *J. Fl. Eng*., **106**, 399-404.
2. Buchlin, J.M., 1997, Modeling of gas-jet wiping, Thin Liquid Films and Coating Processes, *VKI Lecture Series*, von Karman Institute for Fluid Dynamics.
3. Tu, C. V., Wood, D. H., 1996, Measurements Beneath an Impinging Plane Jet, *Exp. Th. Fl. Sc*., **13**, 364-373
4. Phares, D.J., Smedley, G.T., Flagan, R.C., 2000, The wall shear stress produced by the normal impingement of a jet on a flat surface, *J. Fl. Mech*., **418**, 351-375.
5. Reynolds, W.C., 1987, Fundamentals of turbulence for turbulence modelling and simulation, *Lecture Notes for von Karman Institute*, Agard Report 755.
6. Shih, T.H., Liou, W.W., Shabbir, A., Yang, Z., Zhu, J., 1995, A new k-ε Eddy-viscosity model for high Reynolds number turbulent flows- Model development and validation, *Computer Fluids*, **24(3)**, 227-238.
7. Maurel, S., Solliec, C., 2001, A turbulent plane jet impinging nearby and far from a flat plate, *Exp. in Fluids*, **31**, 687-696.
8. Gosset, A., Lacanette, D., Vincent, S., Arquis, E., Gardin, P., LES-VOF simulations of gas-jet wiping: Confrontation to experiments, *to be presented at the 6th European Coating Symposium*, Bradford, Great Britain, 2005.
9. Durbin, P.A., 1995, Turbulence modelling for non-equilibrium flow, *Center for Turbulence Research*, *Annual Research Briefs 1995*, 149-155.
10. Durbin, P.A., 1996, On the k-ε stagnation point anomaly, *Int. J. Heat and Fluid Flow*, **17**, 89-90.
11. Behnia, M., Parneix, S., Durbin, P., 1997, Accurate modeling of impinging jet heat transfer, *Center for Turbulence Research*, *Annual Research Briefs 1997*, 149-164.
12. Patel, V.C., 1965, Calibration of the Preston Tube and Limitations of its Use in Pressure Gradients, *J. Fluid Mech*., **23**, 185-206.
13. Beltaos, S., Rajaratnam, M., 1973, Plane turbulent impinging jets, *J. Hydraulic Research*, **1**, 29-59.
14. P. C. Babu, K. Mahesh, 2004, Upstream entrainment in numerical simulations of spatially evolving round jets, *Phys. Fluids*, **16(10)**, 3699-3705.

15. Thornton, J.A., Graff, M.F., 1976, An analytical description of the jet finishing process for hot-dip metallic coating on strip, *Metallurgical Trans. B*, **7B**, 607-618.
16. Tuck, E.O., 1983, Continuous coating with gravity and jet stripping, *Phys. Fluids*, **26**, 2352-2358.